Majorana Fermions on the Domain Wall of Marginally Twisted Bilayer of Transition Metal Dichalcogenides

Richang Huang*
Department of Physics, The University of Hong Kong, Hong Kong, China and
Department of Physics, Southern University of Science and Technology, Shenzhen, China

Dapeng Yu
Shenzhen Institute for Quantum Science and Engineering, and Department of Physics, Southern University of Science and Technology, Shenzhen, 518055, China
International Quantum Academy, Shenzhen, 518048, China
Guangdong Provincial Key Laboratory of Quantum Science and Engineering, Southern University of Science and Technology, Shenzhen, 518055, China and
Shenzhen Key Laboratory of Quantum Science and Engineering, Southern University of Science and Technology, Shenzhen,518055, China

Wang Yao
Department of Physics, The University of Hong Kong, Hong Kong, China and
HKU-UCAS Joint Institute of Theoretical and Computational Physics at Hong Kong, China
(Dated: March 5, 2024)

We propose to realize two-dimensional superstructures of chiral topological superconductors based on marginally twisted bilayers of transition metal dichalcogenides in proximity to a conventional $s-$wave superconductor. Majorana Fermions arise at domain boundaries of the AB and $A'B'$ stacking domains as a result of the sign flip across the domain wall in the Rashba spin-orbit coupling coefficient at the valence band edge. Unlike previous models that only allow for one Majorana per boundary, each domain wall can host two helical Majorana edge states with the same Majorana polarization, preventing hybridization. This offers a promising new platform for studying Majorana physics.

I. INTRODUCTION

Nowadays a central focus in condensed matter physics is the search for topological states of matter [1–3]. Similar to the well-known quantum Hall state, a chiral topological superconductor with Bogoliubov-de-Gennes (BdG) Chern number $\mathcal{N}$ has a full pairing bulk gap and holds $\mathcal{N}$ topologically protected chiral Majorana Fermions on the boundaries [4]. For the $|\mathcal{N}| = 1$ case, the Majorana edge state has only half the degrees of freedom of usual chiral Fermions, and a Majorana zero mode in the vortex core[5] would obey non-Abelian statistics [6, 7], which makes it potentially valuable for the realization of topological quantum computing [8]. Intensive efforts have been made to search for the chiral topological superconductor in one- and two-dimension. Making use of the proximity effect of a conventional $s-$wave superconductor, many different artificial designs to realize topological superconductor have been proposed and experimentally studied during past years [9–18]. While experimental results have not always been conclusive, the solid theoretical foundations of the field have driven continued progress [19, 20].

Due to the interlayer hybridization and the moiré superlattice effects, layered assembly of two-dimensional materials has provided versatile possibilities to engineer material properties [21]. In marginally twisted bilayer transition metal dichalcogenides (TMDs) of the nearly parallel stacking, it has been shown both theoretically [22–24] and experimentally [25–27] that lattice reconstruction can take place and lead to the formation of alternating AB or $A'B'$ stacking domains (Fig. 1b), as the energy gain from the expanded areas can overcome the energy cost of domain walls, up to a critical angle $\sim 2.5°$. [28]. With the inversion and mirror symmetry breaking, bilayer TMDs of the AB and $A'B'$ stacking configurations are known to feature out-of-plane electrical polarization and Rashba spin-orbit coupling at the valence band edge at the Γ point [29]. AB and $A'B'$ domains have opposite signs for both the electrical polarization and Rashba coefficient, as illustrated in Fig. 1a. This suggests an intriguing possibility to extend the scenario first proposed by Sau et al. [11], where the combination of Rashba spin-orbit coupling, magnetic field and $s-$wave superconducting gap effectively make itself a chiral topological $p-$wave superconductor. With the alternating signs of the Rashba coefficient between the AB and $A'B'$ domains in the marginally twisted bilayer TMDs, , bringing it in proximity to a conventional superconductor and under a magnetic field can lead to superstructures of topological superconductors. We show that this gives the opportunity to engineer Majorana Fermions on the domain wall between AB and $A'B'$ stacking domains. Additionally, we have also studied a similar setup but with do-

* huangrc@connect.hku.hk

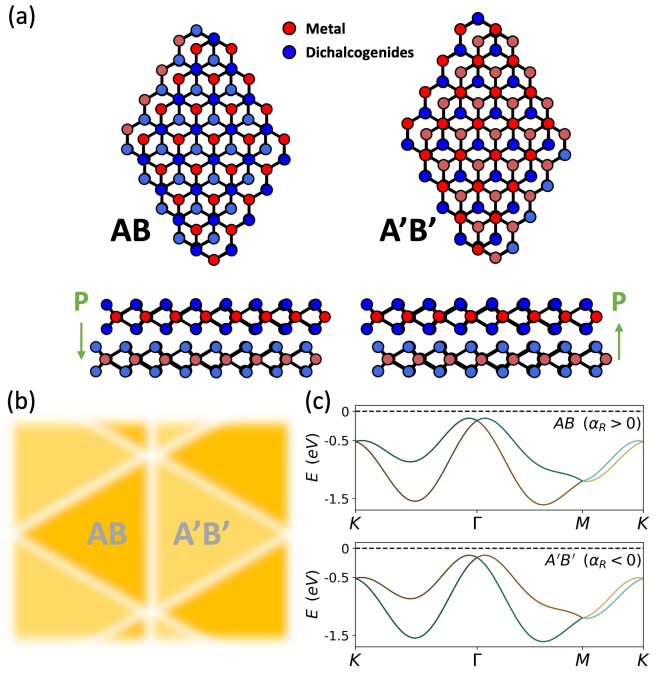

Figure 1. (a) The top and side views of the AB and $A'B'$ stacking configurations of TMD. P indicate the direction of the out out-of-plane electrical polarization arising from inversion and mirror symmetry breaking. (b) Illustration of marginally twisted bilayer transition metal dichalcogenides, where the triangular shape domains of $AB/A'B'$ stacking formed due to lattice reconstruction. (c) Band structures of the AB and $A'B'$ stacking configurations calculated from our tight-binding model with different sign of the Rashba coefficients α_R, where the color green/brown indicate the sign $+/-$ of the spin σ_y of the eigenstates.

main walls between reversed magnetic fields, which could be achieved by placing a ferromagnetic monolayer on an antiferromagnetic substrate [30]. However, as our results show, the chiral edge states in this case are not of the Majorana type.

The organization of this paper is as follows. After this introductory section, Sec. II describes the effective model and parameters we used to simulate the systems. Sec. III provides discussion on the mechanism that prevents the two Majoranas on one domain wall from hybridizing. Sec. IV presents the effects on moiré superlattice. And the last Sec. V concludes the manuscript and gives an outlook.

II. MODEL

The bands in the vicinity of the Fermi energy mainly originate from the $d-$orbitals of the metal atoms. Monolayer TMD has a quasi-2D layered structure consisting of stacked units of metal atoms on a triangular lattice sandwiched between chalcogen elements. But due to the complexity of the structure and the small twisted angle required, a detailed microscopic description of systems becomes unmanageable. Fortunately the essential features of topological superconductivity are insensitive to the specifics of the model and rely solely on the particle-hole symmetry. Therefore we employ a low-energy phenomenological model to describe the domain wall of a marginally twisted bilayer TMD covered by a conventional superconductor and on a magnetic insulator or subjected to an external magnetic field, in which the Zeeman effect and the superconductivity are introduced. We use a 2D tight-binding Hamiltonian, which corresponds to a discretization of the continuous model [11] on a triangular lattice with primitive vectors $\overrightarrow{a_1} = (a, 0)$, $\overrightarrow{a_2} = (\frac{a}{2}, \frac{\sqrt{3}a}{2})$, and lattice constant $a = 1$.

$$\begin{aligned}\mathcal{H} = &-\sum_{i,j,\sigma} t_{ij} c^\dagger_{i\sigma} c_{j\sigma} - \mu \sum_{i,\sigma} c^\dagger_{i\sigma} c_{i\sigma} \\ &+ i\alpha_R(i) \sum_{\langle i,j\rangle,\sigma,\sigma'} \left(x_{ij}\sigma_x - y_{ij}\sigma_y\right)_{\sigma,\sigma'} c^\dagger_{i\sigma} c_{j\sigma'} \\ &+ \sum_{i,\sigma,\sigma'} \left(V_Z(i)\sigma_z\right)_{\sigma,\sigma'} c^\dagger_{i\sigma} c_{i\sigma'} \\ &+ \sum_i \Delta \left(c^\dagger_{i\uparrow} c^\dagger_{i\downarrow} + H.c.\right)\end{aligned} \tag{1}$$

Here $c^\dagger_{i\sigma}$ is the creation operator on site i at location (x_i, y_i) with spin σ. t_{ij} is to the hopping amplitudes between site i and site j. μ is the chemical potential. $\alpha_R(i)$ and $V_z(i)$ are the Rashba spin-orbit coupling and the Zeeman splitting given by the magnetic field, which can both be spatial-dependent in the discussion below. x_{ij} and y_{ij} are the displacement along each direction when hopping from nearest neighborhood $\langle i, j\rangle$. Δ is the induced $s-$wave superconducting pairing. The Kwant package [31] were adopted in part of the numerical calculations performed. Here we note that a model similar to Eq. 1 were used in Ref. [32] to successfully describe the topological superconductivity experimentally discovered in ferromagnet/superconductor heterostructure.

Eq. 1 can actually be mapped to two sets of spinless $p \pm ip-$wave superconductors [33]. Consider a ribbon geometry and take $\Delta_e = \frac{\alpha\Delta}{|V_Z|}$, $\mu_e = |V_Z| - \sqrt{\mu^2 + \Delta^2}$. Assuming $\mu_e = -\mu_0$ is a negative constant for $x < 0$ and $\mu_e = +\mu_0$ is a positive constant for $x > 0$, then one can follow the steps for $p \pm ip-$wave superconductors [34] to find the the Jackiw-Rebbi solution on the emergence of Majorana edge states for this Hamiltonian near the Γ point:

$$\left|\psi_{p_y}(x, y)\right\rangle = e^{ip_y y} \exp\left(-\frac{1}{2|\Delta_e|}\int_0^x \mu_e\left(x'\right) dx'\right) |\phi_0\rangle \tag{2}$$

with a constant spinor $|\phi_0\rangle = 1/\sqrt{2}\begin{pmatrix}1 & 1\end{pmatrix}^T$ acting on one set the effective $p-$wave basis, and the eigenenergy $E(p_y) = -2|\Delta_e|p_y$ showing a gapless, linear and chiral dispersion of the Majorana Fermion. The chirality is de-

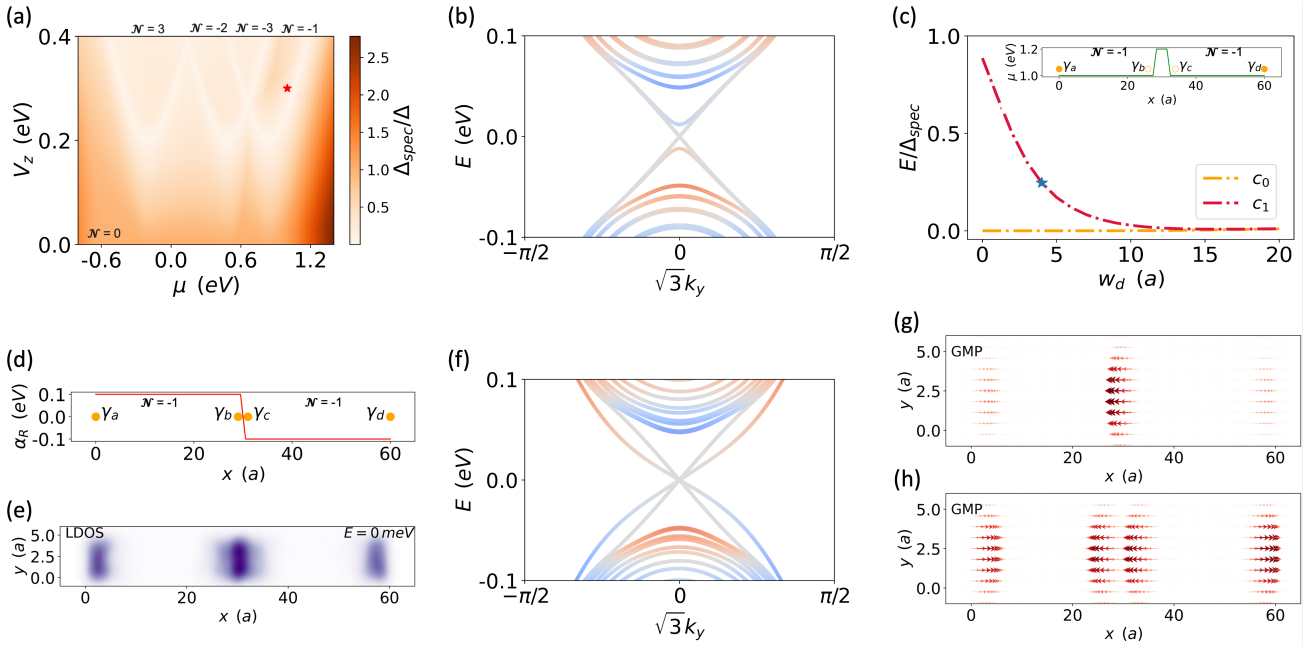

Figure 2. (a) The phase diagram showing the bulk spectrum gap Δ_{spec} of the model for different sets of (μ, V_z) and the associated BdG Chern number $\mathcal{N}$ for each region. The red star indicate the parameters adopted in for the rest of discussion. (b) Spectrum of ribbon with Majorana on boundaries and fused Fermion on domain wall. The color represents the bands are particle-like (blue), hole-like (red) or charge-neutral (grey)(c) Energy of the eigenstates during the process of fusion. The inset shows the profile of the chemical potential domain wall. The solid orange circles represent well established Majoranas while the hollow circles represent fused Fermions.(d) The profile of Rashba domain wall. (e) Zero energy local density of states of the inversed Rashba ribbon. (f) Spectrum of ribbon with domain wall of inversed Rashba coefficient. (g)(h) General Majorana polarization of the two lowest energy states in the inversed Rashba ribbon.

termined by the sign of the BdG Chern number:

$$\mathcal{N} = \frac{1}{2\pi}\iint_{\mathrm{BZ}} \mathbf{\Omega}(\mathbf{k}) \cdot d\mathbf{S} \tag{3}$$

where $\mathbf{\Omega}(\mathbf{k}) = i\left[\left\langle \frac{\partial\psi(\mathbf{k})}{\partial k_x} \mid \frac{\partial\psi(\mathbf{k})}{\partial k_y}\right\rangle - \left\langle \frac{\partial\psi(\mathbf{k})}{\partial k_y} \mid \frac{\partial\psi(\mathbf{k})}{\partial k_x}\right\rangle\right]$ is the Berry curvature.

Though the exact value of each parameter in the model is material dependent, the topological nature does not rely on the fine tuned numbers. As shown in Fig. 1c, we plot the bulk spectrum of our model with $t_1 = -0.03$, $t_2 = -0.1$, $t_3 = -0.01$, which correspond to the nearest, second nearest and third nearest neighbor hopping respectively, and $\mu = 1.0$, $\alpha_R = 0.1$ (all energy scales are in the unit of eV) to mimic the valence band calculated in Ref. [29] of bilayer TMD with Rashba spin-orbit coupling. It should be noted that this tight-bingding model is not able to recover the whole bands calculated by using density functional theory (DFT), but still sufficient to describe the band near the Γ point.

For the heterostructure, in which takes the superconducting gap and the Zeeman splitting into account, we plot the bulk spectrum gap Δ_{spec} in Fig. 2a for different V_z and μ, normalized by $\Delta = 0.2$ and labeled $\mathcal{N}$ of each region which is calculated by the numerical method efficiently [35]. Here we note that this exaggerated value of Δ employed here is to reduce the computational complexity (See Appendix A for details). The gap close, associated with change of $\mathcal{N}$, indicating a topological phase transition. Unlike most of the previous models, here the vanishing of Rashba spin-orbit coupling at M and K points leads to additional gap closing, so that $|\mathcal{N}|$ can take values greater than 1. Detailed discussions about it and the experimental realization of $|\mathcal{N}| = 3$ case can be found in Ref. [32].Here we mainly focused on effects of spatial varying and the inversion of Rashba α_R on Majorana edge states. We adopt $V_z = 0.3$ (corresponding to the red star in Fig. 2a) for the rest discussion so that the Majorana Fermions can emerge due to the band inversion at Γ point.

III. MAJORANAS ON THE DOMAIN WALL

In this section, we investigate the influence of the inversion of Rashba spin-orbit coupling between AB and $A'B'$ stacking domains in marginally twisted TMD by introducing spatially-dependent parameters. Recall that the Majorana bound states always comes in pairs and two Majorana modes can fuse to a fermionic mode when bringing them close. This process is illustrated in Fig. 2c where we manually insert a chemical potential domain wall (corresponding to the $\mathcal{N} = 0$ region) in the center of a topological ribbon geometry with translational invari-

ant along y direction and finite length $L = 60$ along x direction. As the width of the domain wall w_d decreasing, the energy (when $k_y = 0$) of the Majorana pair at outer sides $c_0 = \frac{1}{\sqrt{2}}(\gamma_a + i\gamma_d)$ remains zero while the energy of the Majorana pair located at the domain wall $c_1 = \frac{1}{\sqrt{2}}(\gamma_b + i\gamma_c)$ increases and eventually merges into the bulk. Fig. 2b shows a typical spectrum corresponding to the blue star in Fig. 2c, where the color represents the bands are particle-like (blue) , hole-like (red) or charge-neutral (grey). The hybridized fermionic mode and its particle-hole partner with small energy is also referred as quasi-Majoranas [19].

When the lattice reconstruction take place in the marginally twisted TMD, the moiré supercell is filled by the favored AB and $A'B'$ stacking domains with extremely thin domain walls. For simplicity here we use a step function $\alpha_R(x) = 0.1(x < L/2), -0.1(x \geqslant L/2)$ to imitate the domain wall with opposite Rashba coefficient on each side as shown in Fig. 2d. The zero energy local density of states (LDOS) of the ribbon with periodic boundaries along the y-direction and open boundaries along the x-direction is calculated using the kernel polynomial method [36]. Fig. 2e reveals the emergence of zero energy Majoranas not only on the vertical boundaries but also at the center of the domain wall.

The spectrum of such a ribbon was plotted in Fig. 2f where we can find one pair of Majorana modes with modified dispersion in addition to the original Majorana pair at boundaries possessing linear dispersion. It is worth mentioning that, unlike the more commonly observed chiral Majoranas on the boundaries, the Majorana pair on one domain wall is helical in our scenario, due to the chirality remaining unchanged with the sign flip of the Rashba coefficient, which is verified by calculating $\mathcal{N}(\alpha_R = \pm 0.1) = -1$. Helical Majorana modes can also be accomplished in other platforms like Ref. [16] but in which fine tuned parameters were required.

Trying to illustrate the Majorana nature of these states, we adopt the generalized Majorana polarization [37] (GMP) to visualize the local properties of different edge states appeared in different scenarios. In the Nambu basis $C_i = \left(c_{i\uparrow}, c_{i\downarrow}, c^\dagger_{i\downarrow}, -c^\dagger_{i\uparrow}\right)^T$, we can write down the anti-unitary particle-hole operator as $\mathcal{P} = \sigma_y \tau_y \hat{K}$, where we use $\sigma_{l=x,y,z}$ to denote the Pauli matrices in the spin subspace, $\tau_{l=x,y,z}$ in the particle-hole subspace, and $\hat{K}$ is the complex-conjugation operator. A Majorana by definition should satisfy $\mathcal{P}\gamma = \gamma$ up to an arbitrary phase. Then one can project the operator on site i , $\mathcal{P}_i = \mathcal{P}\hat{r}_i$, and calculate

$$\langle \Psi | \mathcal{P}_i | \Psi \rangle = -2 \sum_\sigma \sigma u_{i\sigma} v_{i\sigma} \tag{4}$$

to characterize local distribution of the GMP for an eigenstate $\Psi = (u_\uparrow, u_\downarrow, v_\downarrow, v_\uparrow)^T$. Note that the expectation values of an anti-unitary operator are in vectors in the complex plane and not gauge invariant so that can not be used to compare between different states as also mentioned in Ref. [37]. Fig. 2g and Fig. 2h plotted the general Majorana polarization of the two degenerate zero energy bound states forming by the four Majoranas, where we can see the GMP on the domain wall are always along the same direction. In a hybridized fermionic mode, the two Majoranas should always have opposite polarization. This is because we can always regard one of them serves as real part and the other serves as imaginary part, in other words there is a $\pi/2$ phase difference between them. This leads to a π phase difference in the complex plane after we applied $\mathcal{P}$ to the states. The inversed α_R leads to the inversion of Majorana polarization so that even though the two Majoranas on the domain wall are spatially strong overlapped, they can maintain the Majorana nature.

An intuitive picture of the emergence of a pair of helical Majorana domain wall can also be seen from the point of stacking one-dimensional topological chains to construct a two-dimensional topological system. Similar to the relation between one-dimensional spinless chains and quantum (anomalous) hall [2], the Hamiltonian for two-dimensional topological superconductor can also be constructed by stacking one-dimensional chains appropriately. When the sign of Rashba flipped, one can always expect α_R effectively equals to zero at the domain wall. Since $\Delta_e = \frac{\alpha\Delta}{|V_Z|}$, the inter-chain pairing also vanishes, leaving a pair of Majoranas on the wall. We provide a more detailed description and visualization in Appendix B.

In contrast, if we inspect the domain wall with inversed Zeeman field on each side, the bound states exhibit a different behavior. The dispersion is plotted in Fig. 3a with enlarged center part shown in Fig. 3b. The BdG Chern number $\mathcal{N}(V_Z = \pm 0.3) = \mp 1$. So that in this case the two Majorana modes on the domain wall would have the same chirality and fuse into a chiral Fermion due to the spatial overlapping (the blue and red lines with a negative group velocity), while the other two Majorana edge states remain degenerate as illustrated in Fig. 3c.

Again we calculated the LDOS of the ribbon. As shown in Fig. 3d and Fig. 3e, the zero energy states only distributed on the boundaries, while the small energy fermionic bound state ($E = 2.5meV$ and its particle-hole partner) concentrated on the center domain wall. We also calculated and plotted the GMP for the lowest and second-lowest states in this case. Aside from the energy, what differs from previous case is that the direction of the Majorana polarization flipped across the domain wall as shown in Fig. 3g. This is consistent with the hybridized fermionic mode we described before.

One may wonder what would happen if we simultaneously invert Rashba and Zeeman fields. Here we note because one can always diagonalize the Hamiltonian Eq. 1 into two blocks with spin + and −, where one block is always trivial and the other can be tuned into topological [38]. In the case of simultaneously inversed Rashba and Zeeman, it is just to make the left half of system spin + topological and the right half of the system spin

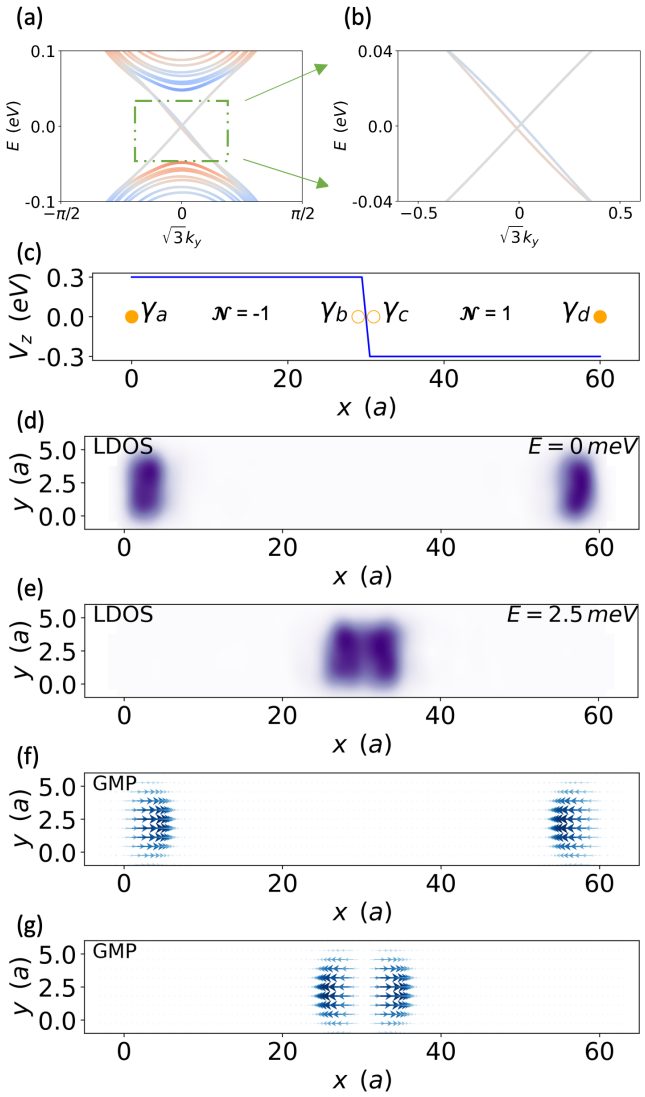

Figure 3. (a) Spectrum of ribbon with domain wall of inversed Zeeman coefficient. (b) Enlarged center part of (a) where a pair of fermionic modes with negative group velocity can be seen clearly. (c) The profile of Zeeman domain wall. (d)(e) Local density of states of the inversed Zeeman ribbon at energy $E = 0$ and $E = 2.5meV$. (f)(g) General Majorana polarization of the two lowest energy states in the inversed Zeeman ribbon.

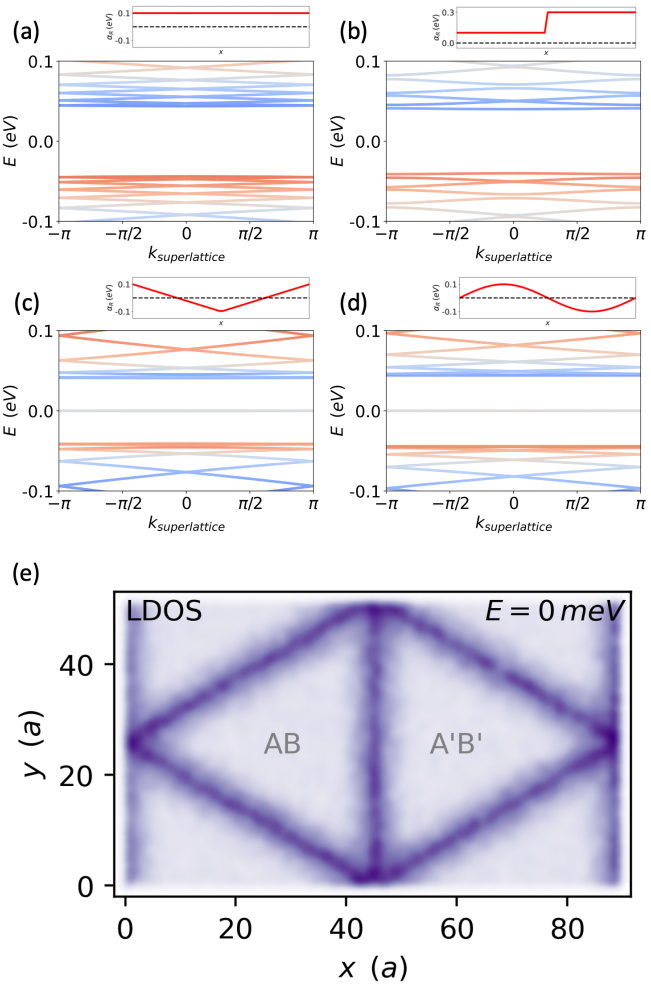

Figure 4. The superlattice dispersion along x direction with (a) homogenous, (b) non inversed step, (c) linearly varying Rashba and (d) sinusoidal Rashba coefficients. (e) The local density of states of a moiré supercell at zero energy.

– topological. Then we have Majorana pair appear on the domain wall, but nothing distinctive would occur.

IV. MAJORANAS ON SUPERLATTICE

Now we investigate the Majorana features on the superlattice in this section. We calculated the dispersion of the one-dimensional superlattice along x direction with the period L corresponding to the previous sections. This setup of superlattice formed by domain walls could be accomplished experimentally by a uniaxial tensile strain on one layer of bilayer TMD to adjust the lattice mismatch [39]. Besides, applying an electric field out-of-plane tends to increase the area of AB or $A'B'$ stacking regions, which is of intensive current interest in the context of sliding ferroelectricity [40]. This implies opportunities for electrical control on the geometry of the Majorana networks.

In addition, we applied different profile of $\alpha_R(x)$, artificially constructed, to confirm that the Majorana bound states are coming from the inversion of the sign of Rashba.

As one can see in Fig. 4a and Fig. 4b, where we set homogeneous Rashba $\alpha_R(x) = 0.1$ and non inversed step Rashba $\alpha_R(x) = 0.1(x < L/2), 0.3(x \geqslant L/2)$, no Majorana are present in the gap of mini Brillouin zone. This helps to confirm that the inversion of Rashba coefficient is the key to harvest Majorana Fermions in our model.

For different varying behavior, as shown in Fig. 4c and Fig. 4d, we set linearly varying Rashba $\alpha_R(x) =$

$-0.4x/L + 0.1(x < L/2), 0.4(x-L)/L + 0.1(x \geqslant L/2)$ and sinusoidal Rashba $\alpha_R(x) = 0.1\sin(2\pi x/L)$. In these cases, every supercell consists of two domain walls (from positive α_R to negative and vice versa) so that two pairs of Majoranas would emerge. And as expected we can see four degenerate Majorana bound states in these two cases (we have checked the four-fold degeneracy of the zero energy states from the numerical data). The Majoranas are dispersionless in this case since they are bounded to the domain wall of Rashba. Comparing the results of these subplots of Fig. 4, we are safe to say the details of profile of $\alpha_R(x)$ has a very limited impact on the topological nature of the emergency of Majoranas.

In Fig. 4e we plot the zero energy local density of states for a (extended) moiré supercell to simulate the marginally twisted TMD. Similar to the ribbon in previous section, the Majoranas concentrate on every domain wall around the triangular AB or $A'B'$ stacking domain as the Rashba coefficient change its sign across the regions. At the crossing points where three identical domain walls intersect, since the domain walls possess the C_3 rotation symmetry, the GMP resided on the domain wall (not always perpendicular to the wall) are also related to each other by C_3 rotation. So that they cancel each other at the crossing points, and we expect no corner states here. We note that if one could introduce a mass term with different signs for the domain walls crossing at one point, the Majorana edge states would be gapped out and Majorana zero modes could survive in the corner [41]. When the triangle size is finite, similar to previous studies on topological states, hybridization would appear. As long as the system size is much larger than the localization length ($\sim \frac{1}{|\Delta_e|}$) the energy resulted from hybridization is exponentially small[42].

V. CONCLUSION AND DISCUSSION

The spatial varying and inversed Rashba spin-orbit coupling features in the marginally twisted TMD. In this manuscript, we extended the well-established model and suggested to realize this new platform on the hybrid system. We have shown that in case of inversed Rashba, the domain wall can host one pair of helical Majorana Fermions when the bulk of the system is in the topological phase. On the contrary, in the case of domain wall with inversed Zeeman or simply a thin topological trivial wall, the associated bound states fused into Fermions.

We also pointed out that the inversion of the Rashba spin-orbit coupling results in the Majorana polarization being the same on both sides, preventing their hybridization. There is a similar analogy in one dimensional nanowires [43], where the so-called Majorana character can save multiple Majorana zero modes at ends of wires. However, it should be noted that the Majorana polarization is not solely determined by the Rashba spin-orbit coupling but is also affected by other parameters such as the phase of the superconducting pairing gap and even the Zeeman field, with complex behavior.

For a realistic system containing a large number of moiré supercells as shown before, the Majorana modes at boundaries would couple to form a network. The shapes of stacking domains, meanwhile the shapes of the network, are not always triangular and can be modified by external factors such as strain or electric fields. In other systems like topological insulator and magnetic topological insulators [39, 44], the interplay between topological edge states and the moiré effects have been carefully studied. Besides edge states, the interplay of the vortices in this scenario may also show a different phenomenon. There are still unfinished works to unveil the manifestation of Majoranas in this context.

ACKNOWLEDGMENTS

This work was supported by the National Key R&D Program of China (2020YFA0309600) and UGC/RGC of Hong Kong SAR (AoE/P-701/20, HKU SRFS2122-7S05), the Shenzhen–Hong Kong cooperation zone for technology and innovation (Contract No. HZQB-KCZYB-2020050), the Innovation Program for Quantum Science and Technology (Grants No. ZD0301703).

Appendix A: Effect of Δ Scaling

In the realm of experimental observations, the conventional superconducting pairing gap typically exhibits a magnitude of a few millielectronvolts, significantly smaller in comparison to other pertinent parameters in our model. In order to achieve an energy resolution capable of discerning details within a few percent of the pairing gap, the computational lattice must possess a linear dimension on the order of thousands sites, which makes the diagonalization process becomes computationally intensive. To address this issue, it is common practice to employ exaggerated values of the pairing gap and assess the reliability of this approach by examining the scaling behavior of the results [32]. Notably, we have verified through calculations performed on larger scales that our findings obtained using exaggerated values indeed faithfully represent the outcomes that would be obtained with a realistic, smaller value of the pairing gap. This seemingly counterintuitive observation aligns with similar findings in one-dimensional systems, where the localization length remains unaffected by variations in the superconducting gap [45].

As demonstrated in Fig. 5, we present the results of scaling down the pairing gap Δ and calculating the spectrum and LDOS for the inversed Rashba ribbon with a linear dimension of L=1000, considering both $\Delta = 0.05$ and $\Delta = 0.005$. These outcomes generally support previous conclusions; however, noticeable irregular oscillations and blurring are observed in the latter case. Employing smaller values of Δ necessitates larger systems and higher

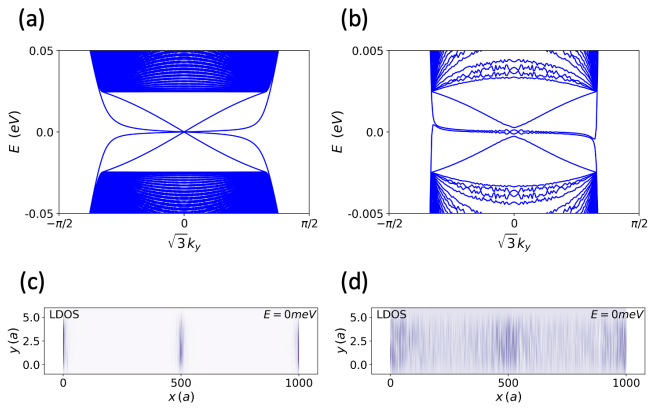

Figure 5. Spectrum of $L = 1000$ ribbon with domain wall of inversed Rashba coefficient and the zero energy local density of states, where $\Delta = 0.05$ in (a)(c) and $\Delta = 0.005$ in (b)(d). All the other parameters are the same as Fig. 2f.

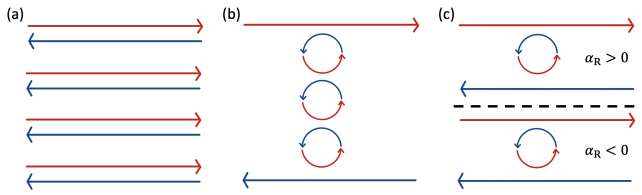

Figure 6. (a) A direct stacking of one-dimensional chains at topological transition point into two-dimensional system. (b) The two-dimensional system can be topological, by setting the inter-chain coupling appropriately. (c) The inter-chain coupling vanishes at Rashba domain wall so that a pair of uncoupled Majoranas are left on the domain wall.

numerical accuracy, which in turn require increased computational resources. Consequently, in the main body of this manuscript, an exaggerated value of Δ is adopted.

Appendix B: Illustration of the Stacking Picture

As we mentioned in Sec. III, similar to the case of quantum hall [2], the two-dimensional topological superconductor can constructed from a stacking of one-dimensional spinless chains but with a different interpretation. In the context of superconductor, the one-dimensional spinless chain is the famous Kitaev chain [46]. When the Kitaev chain is at the topological transition point, it possesses a pair of gapless left moving and right moving modes. One can always stack a bunch of chains to make a two dimensional system. By appropriately choosing the inter-chain coupling terms, one can pair them up into the bulk and left only one mode at each edge. These edge states are protected by the bulk gap and the spatial separation. By doing this, we would obtain the Hamiltonian topological equivalent to the two-dimensional topological superconductor. This process is illustrated in Fig. 6a and Fig. 6b.

Note that the effective pairing term in the model of this manuscript $\Delta_e = \frac{\alpha\Delta}{|V_Z|}$ is proportional to the Rashba coefficient. At the domain wall with flipped α_R, one can always find a place at the domain wall with $\alpha_R = 0$ regardless of the detailed profile of the varying α_R, which leads to the inter-chain coupling vanishes there. So that we can find a pair of helical Majoranas at the domain wall as shown in Fig. 6c.

[1] M. Z. Hasan and C. L. Kane, Reviews of modern physics **82**, 3045 (2010).
[2] X.-L. Qi and S.-C. Zhang, Reviews of Modern Physics **83**, 1057 (2011).
[3] M. Sato and Y. Ando, Reports on Progress in Physics **80**, 076501 (2017).
[4] F. Wilczek, Nature Physics **5**, 614 (2009).
[5] G. Volovik, Journal of Experimental and Theoretical Physics Letters **70**, 609 (1999).
[6] N. Read and D. Green, Physical Review B **61**, 10267 (2000).
[7] D. A. Ivanov, Physical review letters **86**, 268 (2001).
[8] C. Nayak, S. H. Simon, A. Stern, M. Freedman, and S. D. Sarma, Reviews of Modern Physics **80**, 1083 (2008).
[9] R. M. Lutchyn, J. D. Sau, and S. D. Sarma, Physical review letters **105**, 077001 (2010).
[10] Y. Oreg, G. Refael, and F. Von Oppen, Physical review letters **105**, 177002 (2010).
[11] J. D. Sau, R. M. Lutchyn, S. Tewari, and S. D. Sarma, Physical review letters **104**, 040502 (2010).
[12] X.-L. Qi, T. L. Hughes, and S.-C. Zhang, Physical Review B **82**, 184516 (2010).
[13] V. Mourik, K. Zuo, S. M. Frolov, S. Plissard, E. P. Bakkers, and L. P. Kouwenhoven, Science **336**, 1003 (2012).
[14] S. Nadj-Perge, I. K. Drozdov, J. Li, H. Chen, S. Jeon, J. Seo, A. H. MacDonald, B. A. Bernevig, and A. Yazdani, Science **346**, 602 (2014).
[15] J.-P. Xu, M.-X. Wang, Z. L. Liu, J.-F. Ge, X. Yang, C. Liu, Z. A. Xu, D. Guan, C. L. Gao, D. Qian, *et al.*, Physical review letters **114**, 017001 (2015).
[16] J. Wang, Q. Zhou, B. Lian, and S.-C. Zhang, Physical Review B **92**, 064520 (2015).
[17] H.-H. Sun, K.-W. Zhang, L.-H. Hu, C. Li, G.-Y. Wang, H.-Y. Ma, Z.-A. Xu, C.-L. Gao, D.-D. Guan, Y.-Y. Li, *et al.*, Physical review letters **116**, 257003 (2016).
[18] S. Manna, P. Wei, Y. Xie, K. T. Law, P. A. Lee, and J. S. Moodera, Proceedings of the National Academy of Sciences **117**, 8775 (2020).
[19] H. Pan and S. D. Sarma, Physical Review Research **2**, 013377 (2020).
[20] D. I. Pikulin, B. van Heck, T. Karzig, E. A. Martinez, B. Nijholt, T. Laeven, G. W. Winkler, J. D. Watson, S. Heedt, M. Temurhan, *et al.*, arXiv preprint arXiv:2103.12217 (2021).
[21] K. Novoselov, o. A. Mishchenko, o. A. Carvalho, and A. Castro Neto, Science **353**, aac9439 (2016).
[22] M. H. Naik and M. Jain, Physical review letters **121**, 266401 (2018).
[23] S. Carr, D. Massatt, S. B. Torrisi, P. Cazeaux, M. Luskin, and E. Kaxiras, Physical Review B **98**, 224102 (2018).
[24] M. H. Naik, I. Maity, P. K. Maiti, and M. Jain, The Journal of Physical Chemistry C **123**, 9770 (2019).
[25] A. Weston, Y. Zou, V. Enaldiev, A. Summerfield, N. Clark, V. Zólyomi, A. Graham, C. Yelgel, S. Magorrian, M. Zhou, *et al.*, Nature Nanotechnology **15**, 592 (2020).
[26] Z. Zhang, Y. Wang, K. Watanabe, T. Taniguchi, K. Ueno, E. Tutuc, and B. J. LeRoy, Nature Physics **16**, 1093 (2020).
[27] A. Weston, E. G. Castanon, V. Enaldiev, F. Ferreira, S. Bhattacharjee, S. Xu, H. Corte-León, Z. Wu, N. Clark, A. Summerfield, *et al.*, Nature nanotechnology **17**, 390 (2022).
[28] V. Enaldiev, V. Zólyomi, C. Yelgel, S. Magorrian, and V. Fal'ko, Physical Review Letters **124**, 206101 (2020).
[29] Z. Lin, C. Si, S. Duan, C. Wang, and W. Duan, Physical Review B **100**, 155408 (2019).
[30] Q. Tong, F. Liu, J. Xiao, and W. Yao, Nano letters **18**, 7194 (2018).
[31] C. W. Groth, M. Wimmer, A. R. Akhmerov, and X. Waintal, New Journal of Physics **16**, 063065 (2014).
[32] S. Kezilebieke, M. N. Huda, V. Vaňo, M. Aapro, S. C. Ganguli, O. J. Silveira, S. Głodzik, A. S. Foster, T. Ojanen, and P. Liljeroth, Nature **588**, 424 (2020).
[33] J. Alicea, Physical Review B **81**, 125318 (2010).
[34] B. A. Bernevig, *Topological insulators and topological superconductors* (Princeton university press, 2013).
[35] T. Fukui, Y. Hatsugai, and H. Suzuki, Journal of the Physical Society of Japan **74**, 1674 (2005).
[36] A. Weiße, G. Wellein, A. Alvermann, and H. Fehske, Reviews of modern physics **78**, 275 (2006).
[37] N. Sedlmayr and C. Bena, Physical Review B **92**, 115115 (2015).
[38] S.-Q. Shen, *Topological insulators*, Vol. 174 (Springer, 2012).
[39] Q. Tong, H. Yu, Q. Zhu, Y. Wang, X. Xu, and W. Yao, Nature Physics **13**, 356 (2017).
[40] M. Wu and J. Li, Proceedings of the National Academy of Sciences **118**, e2115703118 (2021).
[41] X. Zhu, Physical Review B **97**, 205134 (2018).
[42] P. Marra, Journal of Applied Physics **132** (2022).
[43] N. Sedlmayr, M. Guigou, P. Simon, and C. Bena, Journal of Physics: Condensed Matter **27**, 455601 (2015).
[44] C. Xiao, J. Tang, P. Zhao, Q. Tong, and W. Yao, Physical Review B **102**, 125409 (2020).
[45] D. Sticlet, B. Nijholt, and A. Akhmerov, Physical Review B **95**, 115421 (2017).
[46] A. Y. Kitaev, Physics-uspekhi **44**, 131 (2001).